Draft version March 9, 2024
Preprint typeset using LaTeX style emulateapj v. 12/16/11

arXiv:1805.05875v1 [astro-ph.HE] 14 May 2018

LOW-ENERGY ELECTRONS IN GRB AFTERGLOW MODELS

Guðlaugur Jóhannesson
Science Institute, University of Iceland, Dunhagi 3, 107 Reykjavík, Iceland and
Nordita KTH Royal Institute of Technology and Stockholm University Roslagstullsbacken 23, SE-106 91 Stockholm, Sweden

Gunnlaugur Björnsson
Science Institute, University of Iceland, Dunhagi 3, 107 Reykjavík, Iceland
Draft version March 9, 2024

ABSTRACT

Observations of gamma-ray burst (GRB) afterglows have long provided the most detailed information about the origin of this spectacular phenomena. The model that is most commonly used to extract physical properties of the event from the observations is the relativistic fireball model, where ejected material moving at relativistic speeds creates a shock wave when it interacts with the surrounding medium. Electrons are accelerated in the shock wave, generating the observed synchrotron emission through interactions with the magnetic field in the downstream medium. It is usually assumed that the accelerated electrons follow a simple power-law distribution in energy between specific energy boundaries and that no electron exists outside these boundaries. This work explores the consequences of adding a low-energy power-law segment to the electron distribution whose energy contributes insignificantly to the total energy budget of the distribution. The low-energy electrons have a significant impact on the radio emission, providing synchrotron absorption and emission at these long wavelengths. Shorter wavelengths are affected through the normalization of the distribution. The new model is used to analyze the light curves of GRB 990510 and the resulting parameters compared to a model without the extra electrons. The quality of the fit and the best fit parameters are significantly affected by the additional model component. The new component is in one case found to strongly affect the X-ray light curves showing how changes to the model at radio frequencies can affect light curves at other frequencies through changes in best fit model parameters.

Keywords: gamma-ray burst: general — methods: data analysis — radiation mechanisms: non-thermal

1. INTRODUCTION

Gamma-ray bursts (GRBs) are the most powerful explosions in the Universe and can therefore be observed to very high redshift. They have been hypothesised to be tracers of star formation and thus be a probe of the star formation history of the early universe (Chary et al. 2016). Using the bursts as effective tools in cosmological studies requires a solid understanding of the physics that drives the explosions and the observable consequences of the GRB-events (Wang et al. 2015). Our understanding of GRBs comes mostly through observations of their afterglow emission at wavelengths ranging from radio to X-rays (e.g. Piran 2004; Gehrels et al. 2009). These observations are best interpreted with a model where the emission arises from shocks in a relativistically expanding jet, internal shocks for the prompt high-energy GRB emission and external shocks for the afterglow. Electrons are accelerated to high energies in these shocks giving rise to synchrotron emission as they interact with the magnetic field in the downstream medium.

The theory of particle acceleration in relativistic shocks is far from complete but it is generally acknowledged that a population of high-energy particles form whose distribution can be approximated as a power-law in momentum (Pelletier et al. 2017). These high energy particles contain most of the energy of the distribution and are responsible for the non-thermal emission arising in the model. There are, however, a considerable number of lower energy electrons that can contribute to the long-wavelength emission and increase absorption. Ressler & Laskar (2017) studied the effect of adding a thermal population of electrons to the power-law distribution and find that it can provide significant effects even in the optical frequency range depending on the chosen parameters. Their analysis showed calculated light curves for several models but they did not compare it to any observations to test the validity of the model.

This work also focuses on the effects of low-energy electrons by extending the electron distribution to low energies using a power-law segment. A power-law distribution is chosen over a thermal distribution for simplicity to demonstrate the effect on parameter determination from fitting afterglow observations. A thermal distribution requires at least two parameters and special care to get a continuous distribution while the extra power-law segment requires only a single parameter and the distribution is automatically continuous. The extension is added to the GRB afterglow model of Jóhannesson et al. (2006) that has been used to analyze several GRB afterglows (de Ugarte Postigo et al. 2005, 2007; Resmi et al. 2012; Sánchez-Ramírez et al. 2017). To test the effect of the additional electrons the model is used to analyse the afterglow observations of GRB 990510 that has been well studied (e.g. Panaitescu & Kumar 2001, 2002; Jóhannesson et al. 2006). The results show a statistical preference for models with additional low-energy

gudlaugu@hi.is, gulli@hi.is

electrons indicating the need for further exploration of the electron distribution in GRB afterglow models. The paper is organized as follows: in section 2 the model and the new extension is described and its effects explored, in section 3 the results of the analysis of GRB 990510 are presented and the paper concludes with discussion in section 4.

2. MODEL

The model in Jóhannesson et al. (2006) assumes the afterglow emission arises from a relativistic shock wave traveling through the central engine's surrounding medium. The shock wave is formed as a relativistic slab of matter with energy $E_0 = \Gamma_0 M_0 c^2$ is released into a cone having a half opening angle θ_0. The shock is assumed to accelerate electrons to relativistic speeds and a strong magnetic field is generated within the downstream medium resulting in synchrotron emission. The dynamics of the system is determined from energy and momentum conservation, assuming the downstream medium is a thin uniform shell that expands sideways at the local speed of sound and sweeps up everything in its way (Rhoads 1999). The density of the surrounding medium can have an arbitrary radial dependence but in this work only two forms are considered, a constant density medium, $\rho(r) = m_p n_0$, and a wind-like medium, $\rho(r) = C_w A_* r^{-2}$. Here r is the distance from the central engine, m_p is the mass of the proton, n_0 is the number density of the external medium, A_* is a normalization parameter, and $C_w = 5.015 \cdot 10^{11}\,\mathrm{g\,cm^{-1}}$ for a typical Wolf-Rayet star (Dai & Lu 1998; Chevalier & Li 1999).

The electron energy distribution in this model is based on the one described in Panaitescu & Kumar (2001), but extended to low energies with an additional power-law section. The electron distribution is

$$\frac{dn}{d\gamma} = n_{e,0} \begin{cases} \left(\frac{\gamma}{\gamma_1}\right)^{-p_l}, & \gamma_0 < \gamma < \gamma_1, \\ \left(\frac{\gamma}{\gamma_1}\right)^{-p_c}, & \gamma_1 < \gamma < \gamma_2, \\ \left(\frac{\gamma_2}{\gamma_1}\right)^{-p_c} \left(\frac{\gamma}{\gamma_2}\right)^{-p-1}, & \gamma_2 < \gamma < \gamma_M, \end{cases} \quad (1)$$

where $\gamma_1 = \min\{\gamma_i, \gamma_c\}$, $\gamma_2 = \max\{\gamma_i, \gamma_c\}$, $p_c = p$ in the slow cooling phase where $\gamma_i < \gamma_c$, and $p_c = 2$ in the fast cooling phase with $\gamma_c < \gamma_i$. The lower limit of the distribution is fixed at $\gamma_0 = 2$ because our formalism for the emitting radiation is only valid for high-energy electrons. Here, γ_i is the injection break Lorentz factor which is defined assuming the electrons at the injection break contain a fraction ϵ_i of the total kinetic energy of the downstream medium,

$$\gamma_i = \epsilon_i \frac{m_p}{m_e}(\Gamma - 1) + 1, \quad (2)$$

where m_e is the mass of the electron. The cooling Lorentz factor is,

$$\gamma_c = \frac{4\pi m_e c}{\sigma_T B'^2 t'}, \quad (3)$$

which is found by equating the synchrotron energy loss at time t' with the energy of the electrons (Kardashev 1962). Primed quantities are evaluated in the co-moving rest-frame of the shock wave. Here σ_T is the Thompsons' cross section and $B' = \sqrt{32\pi\epsilon_B \Gamma(\Gamma - 1)\rho c^2}$ is the magnetic field strength.

The energy of the distribution should be dominated by electrons with Lorentz factors above or around γ_1 so $p_l < 2$. For large *negative* values of p_l, the distribution behaves effectively as a distribution without the low energy extension. The normalization factor $n_{e,0}$ is determined from particle conservation. The maximum Lorentz factor γ_M is determined such that the acceleration timescale does not exceed the radiative loss timescale (Dai & Lu 1998) and the total energy of the electron distribution does not exceed a fraction $\epsilon_e < 1$ of the kinetic energy of the downstream medium. Depending on the exact values of the parameters, the latter condition can result in a sharp break in the emitted spectrum above the synchrotron frequency associated with γ_M. This break can even extend down to the optical range or lower at late times for certain parameter values.

The synchrotron radiation is calculated using the standard assumption that the pitch angle between the electrons and the magnetic field is isotropic. The radiation is calculated numerically in the model by integrating the synchrotron power per electron over the electron distribution. Using standard assumptions (e.g. Sari et al. 1998) one can easily derive an approximate power-law behavior for the resulting co-moving frame radiation power

$$P'_\nu(\nu') \propto \begin{cases} \nu'^{1/3}, & \text{if} \quad \nu' < \nu'_l, \\ \nu'^{-(p_l-1)/2}, & \text{if} \quad \nu'_l \le \nu' < \nu'_1, \\ \nu'^{-(p_c-1)/2}, & \text{if} \quad \nu'_1 \le \nu' < \nu'_2, \\ \nu'^{-p/2}, & \text{if} \quad \nu'_2 \le \nu' < \nu'_M. \end{cases} \quad (4)$$

Here ν'_k is the synchrotron frequency corresponding to the Lorentz factor γ_k. It is assumed that $p_l > 1/3$. The additional low-energy electrons therefore contribute to the emitted spectrum for $\nu' < \nu'_1$. The contribution to the synchrotron absorption coefficient can also be evaluated and if $p_l > -2/3$ then

$$\alpha'_\nu(\nu') \propto \begin{cases} \nu'^{-5/3}, & \text{if} \quad \nu' < \nu'_l, \\ \nu'^{-(p_l+4)/2}, & \text{if} \quad \nu'_l \le \nu' < \nu'_1, \\ \nu'^{-(p_c+4)/2}, & \text{if} \quad \nu'_1 \le \nu' < \nu'_2, \\ \nu'^{-(p+5)/2}, & \text{if} \quad \nu'_2 \le \nu' < \nu'_M. \end{cases} \quad (5)$$

The low energy electrons contribute to the absorption of the synchrotron spectrum even in the case their contribution to the emission is insignificant. In addition to the change in spectrum, the low-energy electrons affect the estimation of the normalization constant $n_{e,0}$ and therefore the normalization of the emission at all frequencies. Numerical calculations show that $p_l \lesssim -10$ is required before the effects of the extra component can be completely neglected although the effect is small up to $p_l \lesssim -2$.

The effect of the low-energy extension is illustrated in Figure 1 that shows results of model calculations for several values of p_l. The other parameters are fixed at typical values for GRB afterglows: $E_0 = 10^{51}$ erg, $\Gamma_0 = 1000$, $\theta_0 = 3°$, $n_0 = 1\ \mathrm{cm^{-3}}$, $p = 2.2$, $\epsilon_e = 0.3$, $\epsilon_i = 0.01$, and $\epsilon_B = 0.001$. As expected from the analytical approximations in Eq. (4) the effect is largest for the radio and mm light curves whose frequencies are below ν_i before 10 and 1 days, respectively. The radio light curve is particularly affected because of increased synchrotron self-absorption for $p_l > 0.33$ that shows up in the fast rise of the early radio light curve. The effect on the near-IR

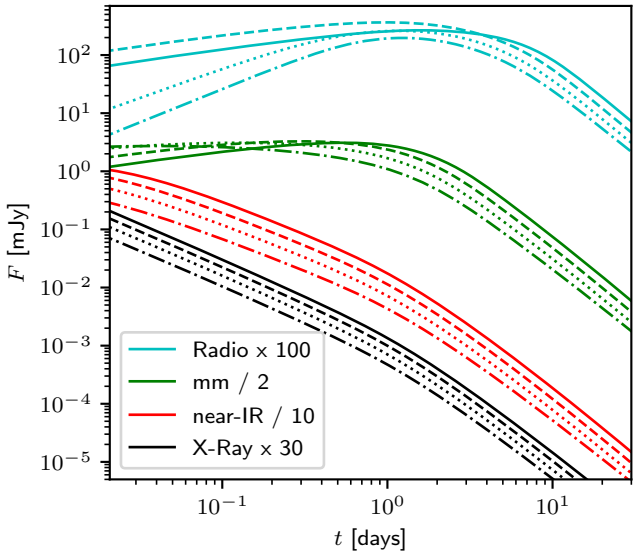


Figure 1. Resulting light curves from example calculations were the value of p_l is varied. Four frequency bands are shown: radio (5 GHz, cyan), mm (100 GHz, green), near-IR (K-band, red), and X-rays (3 keV, black). Four values of p_l are used: -10 (solid curve), -0.66 (dashed curve), 0.33 (dotted curve), and 0.75 (dash-dotted curve).

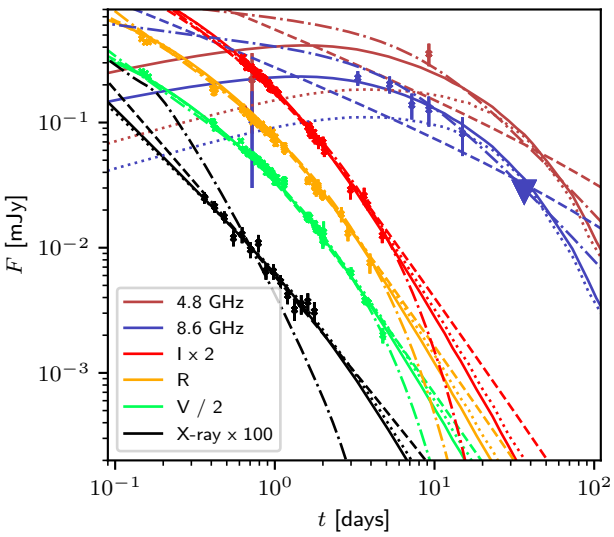


Figure 2. Afterglow light curves of GRB 990510. Data are shown with error bars overlaid with best fit models as curves. CM is solid, CMo is dotted, WM is dashed, and WMo is dash-dotted. Different colors represent different wavebands as illustrated in the legend.

to X-rays is in this case only through the normalization of the light curve. The increased number of electrons at low energies results in lower emission, even though the total energy of the electron distribution is dominated by electrons around γ_i.

3. APPLICATION TO GRB 990510

The afterglow of GRB 990510 has been referred to as the canonical afterglow light curve due to its smooth decline that can be well modeled with synchrotron emission from a collimated shock wave (Stanek et al. 1999; Harrison et al. 1999; Kuulkers et al. 2000; Holland et al. 2000; Panaitescu & Kumar 2001; Jóhannesson et al. 2006). Its afterglow is well sampled with data at many wavelengths from radio to X-rays. The data used in this analysis is from Harrison et al. (1999) (optical and radio), Stanek et al. (1999) (optical), and Kuulkers et al. (2000) (X-rays). The optical data is corrected for Milky-Way dust extinction of E(B-V)=0.2 (Schlegel et al. 1998).

The Bayesian method is used to test the effect of the additional low-energy electrons by comparing the Bayesian factor of models with and without the low-energy component. Models with both a constant density medium (CM, CMo) and a wind-like medium (WM, WMo) are used. The 'o' in the model names stands for without the low-energy electrons. The Bayesian evidence is calculated using MultiNest, which also provides posterior distributions for the free parameters of the model (Feroz & Hobson 2008; Feroz et al. 2009, 2013). The likelihood is calculated assuming the afterglow flux data are sampled from a log-normal distribution which is equivalent to the apparent magnitude being distributed normally. The prior distributions of the parameters are mostly non-informative uniform or log-uniform distributions bounded only by physical constraints of the model. θ_0 is bound from above to be no larger than 90°, ϵ_e and ϵ_B are constrained to be less than 0.5, and ϵ_i is then constrained to be less than ϵ_e. The initial energy release, E_0, is constrained to be less than 10^{52} erg which is about 10% of the energy expected to be released in the gravitational collapse of a massive star. The value of p_l is also constrained to be less than 1 so both the energy and number of electrons in the distribution peaks at around γ_i. Other boundaries are set such that they do not affect the results.

The best fit model is the WM model where the logarithm of the Bayesian evidence is $\log(Z) = -266$. This is considerably higher than the CM model which has $\log(Z) = -280$ giving a value of 10 for the log of the Bayes factor indicating strong evidence. The WM model gives a better fit to the R-band data while the radio data is better fit with the CM model. Other bands are similar for the models and the WM model thus provides a larger Bayesian evidence because the number of points in the R band is much larger than that in radio. The WMo and CMo models result in significantly worse Bayesian evidence than the corresponding WM and CM models. The Bayesian factor between the CM and CMo models is 37 and for WM and WMo it is 189, providing very strong evidence for the addition of the low energy electrons in this analysis.

The best fit model curves are shown overlaid on the data in Figure 2 for all models. Even though the WM model is statistically better, the CM model looks better because it follows the trend of the radio points and the difference in the R-band is barely visible. It is also clear that the WMo model provides a poor fit to the X-ray data. The low-energy electrons thus significantly affect the quality of the fit at X-ray wavelengths through changes in the model parameters even though they do not contribute to the emission at those wavelengths. It also demonstrates how important multi-wavelength data is for model selection.

The 1D marginal posterior distributions for the model parameters are shown in Figure 3 for the models considered in the analysis. Table 1 shows the parameters posterior mean values, the 68% confidence regions, and

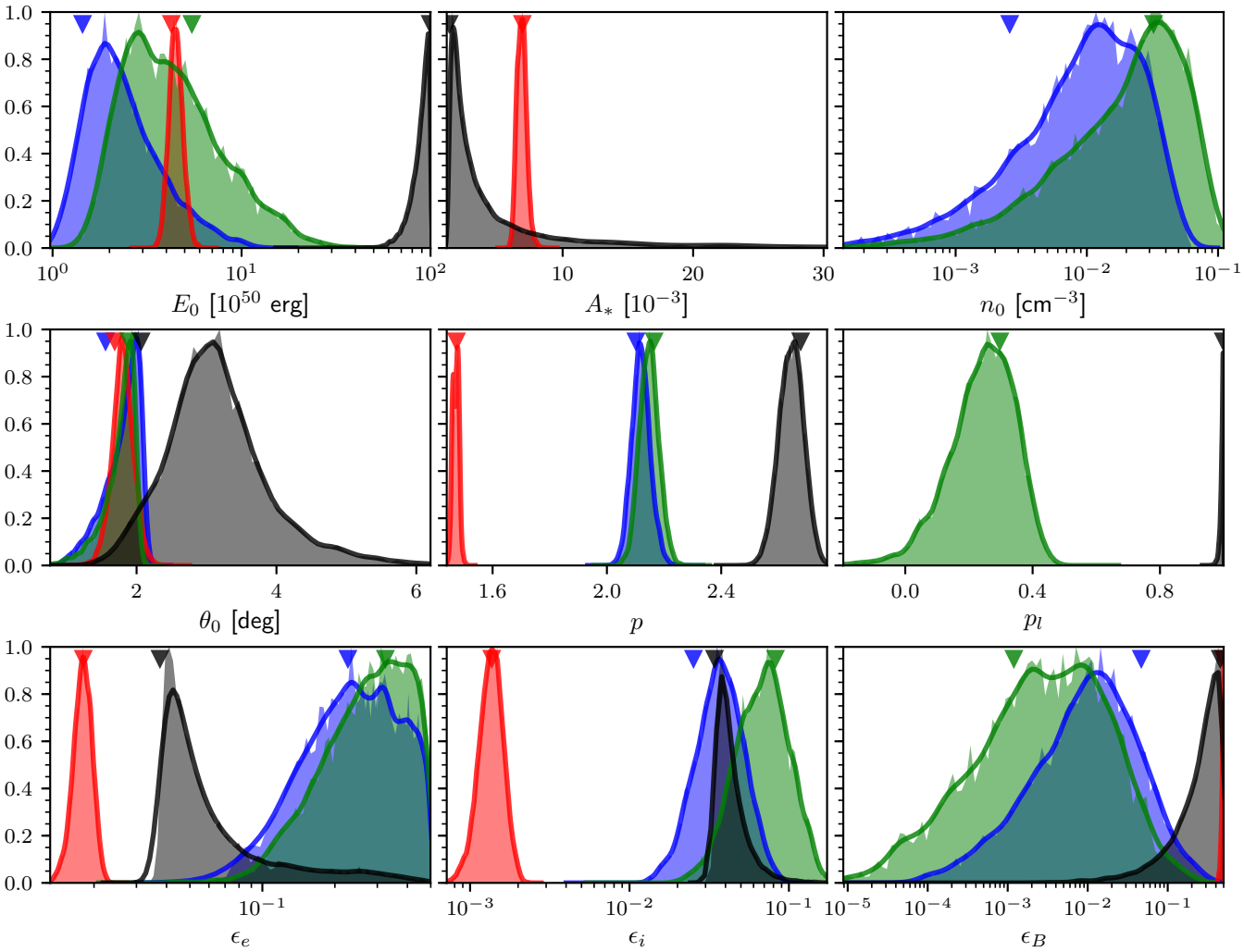


Figure 3. Marginalized posterior distributions for the parameters of the afterglow tuned to the data of 990510 shown in Figure 2. The distributions are normalized to 1 at the peak. Shown are both the actual sampled distributions as half-transparent colors and the Gaussian kernel density estimate as smooth curves. CM is green, CMo is blue, WM is black, and WMo is red. The best fit values used for the model curves in Figure 2 are shown as symbols at the top of the panels. Note that the best fit values are not always near the peak of the distribution.

the maximum likelihood values. The WM model clearly stands out and the posterior distributions are often cut off abruptly by the prior range. The WM model requires large values for the initial energy release, E_0, which is only constrained by the selection of prior. Increasing the size of the prior results in the best fit model having even higher values of E_0 which are beyond reasonable estimates of the available energy from the central engine. The posterior distribution for p_l is also at the boundary set by the prior. Because of these extreme parameter values and the fact that the CM model better reproduces the radio data the CM model is considered a better model of this event even though the WM model is statistically favored.

There is considerable difference between the posterior distributions of the models with and without the low-energy electrons, in particular for the WM and WMo models. The posterior distributions for the WM and CM models are broader compared to the WMo and CMo counterparts and the means of the distributions are also shifted. The effect differs somewhat between the CM and WM models in detail, but the shift is in all cases in the same direction except for the external density. There is a decrease in the posterior mean for A_* in the WM model compared to the WMo model while n_0 is increased in the CM model compared to the CMo model. The 2D marginal posterior distributions (not shown) indicate that p_l is in both models well constrained and there is very little correlation between p_l and the other model parameters.

4. DISCUSSION AND SUMMARY

The best fit model parameters presented here are in reasonable agreement with previous analysis. Panaitescu & Kumar (2001) used a CMo model very similar to the one used in this analysis. Their best fit values are all within the 99% confidence intervals of our posterior distributions apart from the value of θ_0. Their value for θ_0 is 2.7° which is considerably off the posterior distribution determined here. A follow up study was performed in Panaitescu & Kumar (2002) where the parameters changed significantly. In particular their value of θ_0 and n_0 are larger and both outside the posterior distributions presented in Figure 3. Their value of p is also consider-

Table 1
Resulting posterior mean values with the associated 68% confidence intervals for the model parameters. Number in parentheses is the value associated with the maximum likelihood used to create the model curves in Figure 2.

Parameter	CMo	WMo	CM	WM
Bayesian evidence	-317.3 ± 0.4	-454.81 ± 0.03	-280.01 ± 0.03	-265.6 ± 0.2
Minimum χ^2	549.8	814.7	470.1	444.1
E_0 [10^{50} erg]	$2.65^{+1.5}_{-0.66}$ (1.44)	$4.54^{+0.41}_{-0.35}$ (4.25)	$5.3^{+4.1}_{-1.6}$ (5.5)	$89.5^{+6.0}_{-11}$ (99.6)
A_* [10^{-3}]	...	$6.87^{+0.36}_{-0.36}$ (6.91)	...	$2.83^{+1.7}_{-0.50}$ (1.31)
n_0 [cm^{-3}]	$0.0134^{+0.015}_{-0.0075}$ (0.0026)	...	$0.028^{+0.029}_{-0.018}$ (0.032)	...
θ_0 [deg]	$1.79^{+0.17}_{-0.34}$ (1.56)	$1.80^{+0.15}_{-0.15}$ (1.69)	$1.75^{+0.13}_{-0.28}$ (1.89)	$3.15^{+0.70}_{-0.60}$ (2.07)
p	$2.119^{+0.032}_{-0.032}$ (2.101)	$1.471^{+0.011}_{-0.012}$ (1.474)	$2.148^{+0.034}_{-0.034}$ (2.165)	$2.645^{+0.042}_{-0.044}$ (2.678)
p_l	...	...	$0.241^{+0.091}_{-0.11}$ (0.297)	$0.9943^{+0.0030}_{-0.0062}$ (0.9989)
ϵ_e	$0.30^{+0.13}_{-0.12}$ (0.23)	$0.0181^{+0.0016}_{-0.0016}$ (0.0181)	$0.29^{+0.13}_{-0.11}$ (0.32)	$0.0757^{+0.050}_{-0.0094}$ (0.0376)
ϵ_i	$0.039^{+0.015}_{-0.011}$ (0.025)	$0.00137^{+0.00024}_{-0.00023}$ (0.00137)	$0.073^{+0.031}_{-0.024}$ (0.082)	$0.0478^{+0.015}_{-0.0058}$ (0.0342)
ϵ_B	$0.0232^{+0.031}_{-0.0086}$ (0.0467)	$0.4818^{+0.0096}_{-0.021}$ (0.4971)	$0.0103^{+0.015}_{-0.0026}$ (0.0012)	$0.28^{+0.14}_{-0.17}$ (0.45)

ably smaller, but with large uncertainties and agrees with the posterior at the 2σ level. Like the present analysis, Panaitescu & Kumar (2002) find that a constant density external medium better fits the data. This afterglow data was also analysed by Jóhannesson et al. (2006) using an older version of the code used here and a different fitting technique. As expected, the parameter estimates all fall within the 68% confidence intervals of the current posterior distributions.

The results of the analysis of GRB 990510 and the statistical preference for the additional electron component lend support to the need for more detailed treatment of the electron distribution in GRB afterglow modeling. This can in particular affect the determination of the energetics of the outflow and the density structure of the external medium. The power-law segment added in this work is just a simple modification of the electron energy distribution to explore its effects and further work is needed to get a more accurate physical picture. One such method is to simultaneously solve for the dynamics of the afterglow and the distribution of electrons. This was done in the work of (Geng et al. 2018) but their approach is limited to electron cooling and lacks the thermalization effect of the electrons that may be important for the lowest energy electrons. They also excluded several important effects, such as the EATS. Clearly, there is room for considerable improvements in this area of GRB afterglow modeling.

REFERENCES

Chary, R., Petitjean, P., Robertson, B., Trenti, M., & Vangioni, E. 2016, Space Sci. Rev., 202, 181
Chevalier, R. A., & Li, Z.-Y. 1999, ApJ, 520, L29
Dai, Z. G., & Lu, T. 1998, MNRAS, 298, 87
de Ugarte Postigo, A., Castro-Tirado, A. J., Gorosabel, J., et al. 2005, A&A, 443, 841
de Ugarte Postigo, A., Fatkhullin, T. A., Jóhannesson, G., et al. 2007, A&A, 462, L57
Feroz, F., & Hobson, M. P. 2008, MNRAS, 384, 449
Feroz, F., Hobson, M. P., & Bridges, M. 2009, MNRAS, 398, 1601
Feroz, F., Hobson, M. P., Cameron, E., & Pettitt, A. N. 2013, ArXiv e-prints, arXiv:1306.2144
Gehrels, N., Ramirez-Ruiz, E., & Fox, D. B. 2009, ARA&A, 47, 567
Geng, J.-J., Huang, Y.-F., Wu, X.-F., Zhang, B., & Zong, H.-S. 2018, ApJS, 234, 3
Harrison, F. A., Bloom, J. S., Frail, D. A., et al. 1999, ApJ, 523, L121
Holland, S., Björnsson, G., Hjorth, J., & Thomsen, B. 2000, A&A, 364, 467
Jóhannesson, G., Björnsson, G., & Gudmundsson, E. H. 2006, ApJ, 647, 1238
Kardashev, N. S. 1962, Soviet Ast., 6, 317
Kuulkers, E., Antonelli, L. A., Kuiper, L., et al. 2000, ApJ, 538, 638
Panaitescu, A., & Kumar, P. 2001, ApJ, 554, 667
—. 2002, ApJ, 571, 779
Pelletier, G., Bykov, A., Ellison, D., & Lemoine, M. 2017, Space Sci. Rev., 207, 319
Piran, T. 2004, Reviews of Modern Physics, 76, 1143
Resmi, L., Misra, K., Jóhannesson, G., et al. 2012, MNRAS, 427, 288
Ressler, S. M., & Laskar, T. 2017, ApJ, 845, 150
Rhoads, J. E. 1999, ApJ, 525, 737
Sánchez-Ramírez, R., Hancock, P. J., Jóhannesson, G., et al. 2017, MNRAS, 464, 4624
Sari, R., Piran, T., & Narayan, R. 1998, ApJ, 497, L17
Schlegel, D. J., Finkbeiner, D. P., & Davis, M. 1998, ApJ, 500, 525
Stanek, K. Z., Garnavich, P. M., Kaluzny, J., Pych, W., & Thompson, I. 1999, ApJ, 522, L39
Wang, F. Y., Dai, Z. G., & Liang, E. W. 2015, NewAR, 67, 1